NUMERICAL INVESTIGATION OF THE UNSTART SUPPRESSION IN A SUPERSONIC AIR INTAKE[*]

M.R. SOLTANI[**1], J. SEPAHI YOUNSI[2] AND V. FARAJPOOR KHANAPOSHTANI[3]

[1, 2]Dept. of Aerospace Engineering, Sharif University of Technology, Tehran, I. R. of Iran
Email: msoltani@sharif.edu
[2, 3]Mesbah Research Institute, Tehran, I. R. of Iran

Abstract– The starting behavior of a supersonic axisymmetric mixed compression air intake was numerically investigated. The code solves Reynolds-averaged Navier–Stokes equations using an explicit finite volume method in a structured grid by the Roe flux difference splitting scheme. Further, it uses the Baldwin–Lomax algebraic model to compute the turbulent viscosity coefficient. The correct method of surveying the intake starting problem and effects of several geometrical parameters such as: intake throat area, cowl lip roundness and spike surface curvature upstream of the throat on the starting and performance of the intake were studied. Results showed that correct combinations of the mentioned parameters can suppress the intake unstart problem and in addition can prevent the reduction of the intake efficiency.

1. INTRODUCTION

Supersonic air intake as the first component of a supersonic engine has an important role in the engine operation. Type and efficiency of the supersonic air intake have significant effects on the maneuvering capability and efficiency of the propulsion system. Among all types of the supersonic air intake, mixed compression intake (in which compression occurs both outside and inside the intake) is very important due to its special advantages such as low external cowl lip drag and maximum mass flow rate. However; mixed compression intake has some drawbacks such as the starting problem and a smaller margin of the intake buzz.

At the design condition of this type of intake, there exist at least two oblique shocks, one external and one inside the intake that terminates to a normal shock somewhere along the intake, Fig. 1a. The unstarting situation in mixed compression intakes occurs when the normal shock is placed outside the intake, Fig. 1b. At the beginning of the flight when the free stream Mach number is lower than the design Mach number, if the intake is not designed to swallow the normal shock, the unstart condition will occur. In addition, at any time during the flight the unstart problem may take place if the normal shock inside the mixed compression intake is expelled out due to various reasons such as the intake back pressure fluctuations, etc.

At the unstart condition the intake performance will fall down due to the significant reduction of the intake efficiency and mass flow spillage, both of which will result in a high intake drag force. In addition, shock oscillation in front of the intake or buzz phenomenon may occur at this situation which causes unsteadiness in the intake pressure and mass flow rate and may even extinguish the combustion process in the combustor. Therefore, it is important to design the supersonic intake such that it starts at the design point and is able to suppress the unstart phenomenon as much as possible during its operation.
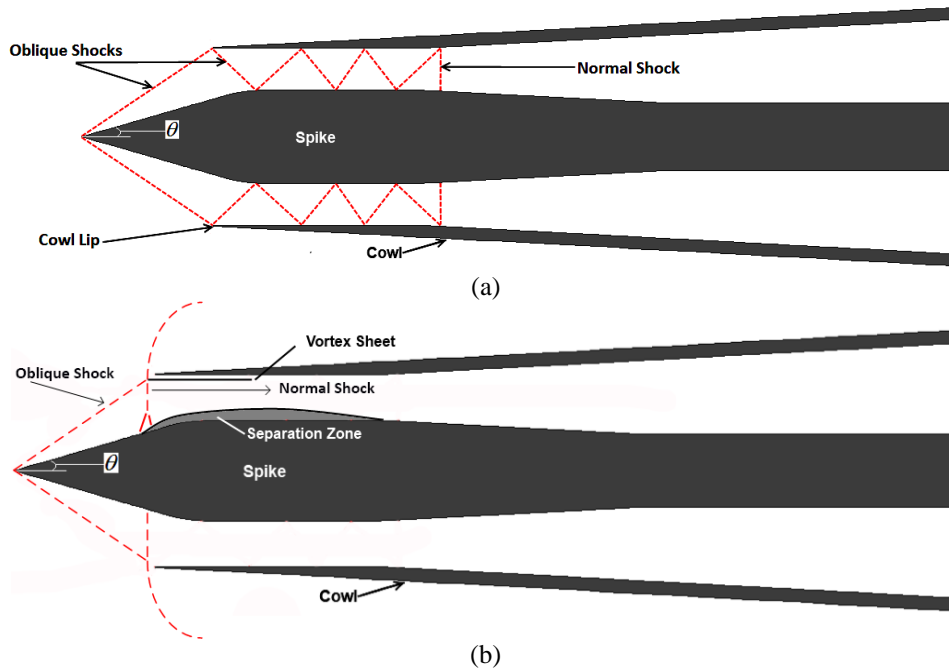
Fig. 1. Intake Geometry and Shock Pattern, a) at Start (Design) Condition, b) at Unstart Condition

To overcome the aforementioned difficulty in these types of intake, several methods such as overspeeding the inlet air momentarily (flying at a Mach number greater than the design Mach number until the normal shock is swallowed by the intake and then reducing the flight Mach number to the design value), varying the intake geometry (especially increasing the intake throat area), and the perforated intake concept are proposed [1-2]. In addition, bypass doors and bleed systems are applied to control the starting characteristics of the supersonic air intake [3-4].

The starting problem has been widely investigated by many researchers due to its importance. Das and Prasad [5-8] performed numerical and experimental simulations of the flow field in a supersonic mixed compression rectangular intake at a free stream Mach number of 2.2. They studied effects of the bleed and cowl bending on the performance and starting characteristics of the intake and showed that these factors can improve the flow quality and performance of the intake and are necessary for starting of the intake.

Kubota et al. experimentally investigated the starting characteristics of a ramp compression type intake at a Mach number of 4.0 and showed that a geometrically bent cowl can improve the starting behavior of the intake [9]. The bend will weaken the shocks and as a result shock induced separation in the intake duct that reduces the internal contraction ratio will be postponed which will avoid choking at the throat. They also showed that the ratio of the height of the intake duct to the boundary layer thickness affects the intake starting characteristics.

Jain and Mittal [10] studied effects of the intake back pressure and ramp geometry close to the throat on the starting characteristics of a mixed compression intake at a free stream Mach number of 3.0 using a two dimensional Euler numerical solver. However, according to the Das and Prasad research [5-6] using an inviscid numerical solver may result in an incorrect result about the starting problem of the intake when compared with the experimental results. In addition, Kotteda and Mittal [11], Sanders and Mitchell [12], Najafiyazdi [13], Slater and Saunders [14] and Nori [15] also investigated various aspects of the supersonic intake starting problem.

The model under investigation in this study is an axisymmetric mixed compression intake that has been designed for a free stream Mach number of 2.0. Its schematic is shown in Fig. 1a. As mentioned

before, in this type of supersonic intake the compression process occurs via oblique shocks outside and inside the intake which are terminated with a normal shock inside the intake, Fig.1a.

To investigate the starting problem of the intake, a numerical code was used. This code has been developed by the authors especially for supersonic intakes and has been throughly validated with the experimental data of a similar supersonic intake. The effects and sensitivity of the intake throat area, cowl lip roundness and spike surface curvature upstream of the throat have been investigated using this code. In addition, in this research the correct method of surveying the intake starting problem by a numerical code will be explained. To the authors' knowledge, this subject and effects of the cowl lip roundness have rarely been studied by the researchers and there seems to be a gap in our knowledge of the mixed compression intakes. Also, various intake performance parameters such as efficiency (TPR: Total Pressure Recovery), FD (Flow Distortion) and MFR (Mass Flow Ratio), in addition to the starting problem, are further investigated.

2. NUMERICAL METHODOLOGY AND CODE VALIDATION

A RANS code that was already developed by the authors and validated with a similar problem was used [16-18]. To construct a suitable grid inside and around the intake, the physical domain is divided into three blocks as shown in Fig. 2. In each block a structured grid was generated using an elliptic grid generator. In this grid generator a system of elliptic partial differential equations are numerically solved to find locations of the grid points [19]:

$$\begin{cases} \xi_{xx} + \xi_{rr} = 0 \\ \eta_{xx} + \eta_{rr} = 0 \end{cases}.$$ (1)

where ξ and η represent coordinates in the computational domain and x and r represent coordinates in the physical domain. To find the location of the grid points, the above system of equations was solved numerically for x and r. The structured grid can easily be refined and stretched in all or part of the physical domain. The entire intake grid is shown in Fig. 3.
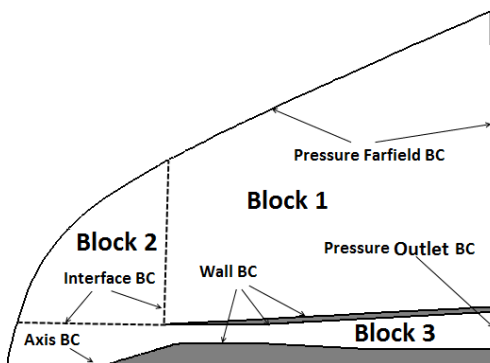

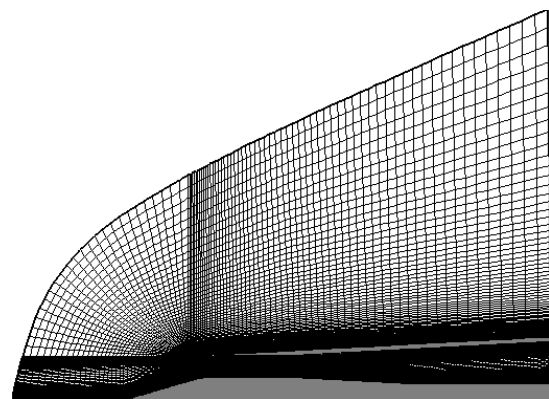Fig. 2. Computational blocks and boundary conditions used in the numerical code

Fig. 3. The Structured Grid Inside and Around the Intake

Neglecting the body forces and any heat addition or extraction, RANS equations in terms of the mean flow quantities in two dimensional (planar and axisymmetric) conservative form are [16-18]:

$$\frac{\partial}{\partial t} \iint_A \vec{W} dA + \int_s \vec{F}_c ds + \alpha \iint_A \vec{V}_c dA = \int_s \vec{F}_v ds + \alpha \iint_A \vec{V}_v dA,$$ (2)

where

$$\vec{W} = \begin{bmatrix} \rho \\ \rho u \\ \rho v \\ \rho E \end{bmatrix}, \vec{F}_c = \begin{bmatrix} \rho V_n \\ \rho u V_n + n_x P \\ \rho v V_n + n_r P \\ \rho H V_n \end{bmatrix}, \vec{F}_v = \begin{bmatrix} 0 \\ n_x \tau_{xx} + n_r \tau_{xr} \\ n_x \tau_{xr} + n_r \tau_{rr} \\ n_x \Theta_x + n_r \Theta_r \end{bmatrix},$$

$$\vec{V}_c = \frac{1}{r} \begin{bmatrix} \rho v \\ \rho u v \\ \rho v^2 \\ \rho v H \end{bmatrix}, \vec{V}_v = \frac{1}{r} \begin{bmatrix} 0 \\ \tau_{xr} \\ \tau_{rr} - \tau_{\theta\theta} \\ u\tau_{xr} + v\tau_{rr} + k\dfrac{\partial T}{\partial r} \end{bmatrix},$$

(3)

and

$$V_n = \vec{V}.\vec{n} = n_x u + n_r v, n_x = \frac{\Delta r}{\Delta s}, n_r = -\frac{\Delta x}{\Delta s}, \Delta s = \sqrt{\Delta x^2 + \Delta r^2},$$

$$\Theta_x = u\tau_{xx} + v\tau_{xr} + k\frac{\partial T}{\partial x}, \Theta_r = u\tau_{xr} + v\tau_{rr} + k\frac{\partial T}{\partial r}.$$

(4)

The vectors $\mathbf{F_c}$ and $\mathbf{F_v}$ in equation (2) are convective and viscous fluxes, respectively, If $\alpha=0$ these equations are for two dimensional planar and if $\alpha=1$ they are for axisymmetric flows. A is the area of the two dimensional cell, Δs is the length of the cell face and V_n is the velocity component normal to the cell face. The equation of state which is used as an auxiliary equation is:

$$P = \rho R T .$$

(5)

By the explicit finite volume discretization method, equation (2) becomes:

$$W_{i,j}^{n+1} = W_{i,j}^n - \frac{\Delta t_{i,j}}{A_{i,j}} [\sum_{k=1}^{4}(F_c)_k \Delta s_k]_{i,j} - \alpha \Delta t_{i,j} V_{c\,i,j} + \frac{\Delta t_{i,j}}{A_{i,j}}[\sum_{k=1}^{4}(F_v)_k \Delta s_k]_{i,j} + \alpha \Delta t_{i,j} V_{v\,i,j}.$$

(6)

The flow is steady and the time derivative term in equation (6) is used to update the flow variables after each iteration until the steady state solution is achieved. To accelerate the convergence, the time step, $\Delta t_{i,j}$, is calculated using the local time stepping method [16-18].

Flux vectors, $\mathbf{F_c}$ and $\mathbf{F_v}$, must be evaluated at the cell face in equation (6). In this research, the convective fluxes are computed by the Roe's scheme and the viscous fluxes are calculated by a finite volume method which is consistent with the overall discretization method [16-18]. Roe's scheme is the most popular scheme in the Flux Difference Splitting, FDS, family and was widely explained in the literature. This scheme was implemented in the numerical code with Harten's entropy correction and MUSCL (Monotone Upstream-Centered Schemes for Conservation Laws) approach was used to increase the spatial accuracy of the discretization using reference [20]. However, higher orders of spatial discretization did improve the results significantly as seen from the code validation graphs. Consequently, first order was used in the numerical code to reduce the time required for the code convergence. Since the problem is steady, the time discretization is also of first order accuracy.

Figure 2 shows the boundary conditions that are used in the present code. The stress terms in the RANS equations are computed by the following viscosity coefficient:

$$\mu = \mu_L + \mu_T ,$$

(7)

where μ_L and μ_T are the laminar and the turbulent viscosity coefficients, respectively. The laminar viscosity coefficient is the molecular viscosity and in this research it is computed from the Sutherland law. The turbulent viscosity coefficient, however, has been calculated by the Baldwin-Lomax turbulence model. This algebraic model is based on the Cebeci–Smith model with some modifications to avoid the

need for locating the edge of the boundary layer. This simple and numerically efficient model has been successfully and widely used for the numerical computation of the flow field in both external and mixed compression intakes [21-25]. In all cases examined in this investigation, there is no serious flow separation and according to the aforementioned references, especially reference [24], the Baldwin-Lomax model can precisely calculate the turbulent viscosity coefficient for flows with no or moderate separation.

Grid resolution study was conducted to ensure that the numerical solution is independent of the grid size. The results showed that a grid with 60×80 points in block 1, 25×80 in block 2, and 300×60 points in block 3 is sufficient and gives accurate results (the left number is the number of nodes in the *x* direction and the right number is the number of nodes in the *r* direction). All grids were generated by an elliptic grid generator that had uniformity in both the grid size and small values of the grid distortion. These characteristics will improve accuracy of the numerical solution significantly [16-18]. Furthermore, it is well known that successful computations of the turbulent flows require special consideration of the mesh generation. This is caused by the strong interaction of the mean flow and turbulence. Therefore, numerical results for the turbulent flows tend to be more grid dependent than those for the laminar flows. Since there exists viscous sublayer near the wall for $y^+ < 2 \sim 8$, it is recommended that the first node (or cell centroid) should be located at a distance $y^+ \leq 1$ from the wall [20]. However, a higher y^+ could be acceptable as long as it is make sure that this value is well inside the viscous sublayer.

In this research a sufficiently fine grid near the walls by means of grid clustering functions was generated such that y^+ was in the desirable range. Comparisons of the numerical and the experimental boundary layer profiles showed that both the turbulence model as well as the grid quality near the wall were acceptable.

The above described numerical methodology has been validated by the wind tunnel test results of a similar supersonic intake [16-18]. The intake that is shown in Fig. 4 is also of axisymmetric one, and is designed for a Mach number of two. However, it is an external compression intake but the overall flow fields are very similar.

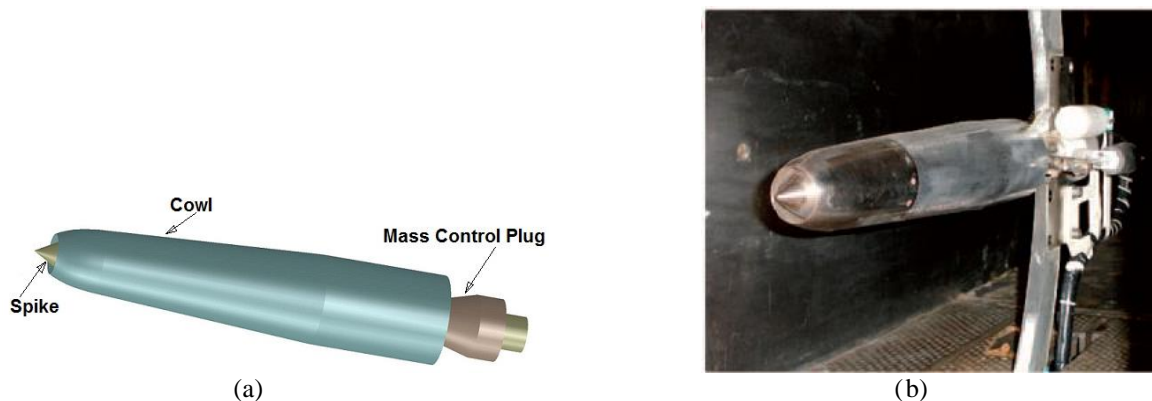| (a) | (b) |

Fig. 4. Intake Used for the Code Validation [18], a) Schematic View, b) Mounted in the Test Section

All experiments were performed in a continuous supersonic wind tunnel; $0.4 \leq M_\infty \leq 3$, with a rectangular test section size of 60×60 cm^2 [16]. The turbulence intensity of the flow in the test section ranges from 0.4% to 1.4%, depending on the freestream Mach number [26-27]. There exist porous bleed holes on the upper and lower walls of the test section that can stabilize and control shock and other reflected waves. The glass windows in the sidewalls of the wind tunnel allow observation of the flow pattern over the nose of the model via the Schlieren and shadowgraph systems. A shadowgraph system and a high speed camera with speed of 1000 frames/second were used in this investigation. The tunnel is of an indraft type; therefore, total pressure and total temperature in the test section are constant, about 85 kPa and 288 k, respectively. The validation intake is an axisymmetric external compression one with an

L/d (length/diameter) of 4.8. The design Mach number of the model is two, and the nose apex semi angle is 28°. The mass flow rate passing through the intake can be varied via a plug located at the end of the model [16]. The model was installed using a C type-mechanism at the mid-section of the wind tunnel.

The cowl and spike surface static pressure distributions in the wind tunnel tests were measured via several sensitive pressure transducers located at different positions. In addition, two boundary layer rakes, one (outer) at *x/d*=4 (*x* is measured from the tip of the spike) located on the cowl surface and another (inner) located on the spike surface at the end of the intake were used to verify the capability of the numerical code in capturing the boundary layer and turbulent phenomena. To reduce the experimental errors (such as the instrumentation calibration, pressure transducers, data acquisition system, system noise and human errors) each test was performed several times and the maximum total experimental error in the pressure measurements was about 1.5% [16-18].

Figure 5 shows comparison of the numerical and experimental values for several flow quantities in various locations as well as the shock pattern of the validation intake (Fig. 4). As seen from this figure good agreements between the numerical and experimental results are achieved. The inaccuracy seen in the inner rake data, Fig. 5d, is mostly due to the presence of the model struts that are not considered in the 2-D axisymmetric computational model. Based on the aforementioned results, the authors were encouraged to extend the existing code in such a way to study the starting problem of a similar supersonic intake, but of mixed compression one. Both intakes are axisymmetric and have been designed for a freestream Mach number of two, however, the validation intake was of external compression type with an *L/d* (length/diameter) of 4.8 while the intake under investigation is a mixed compression one with an *L/d* (length/diameter) of 3.4.
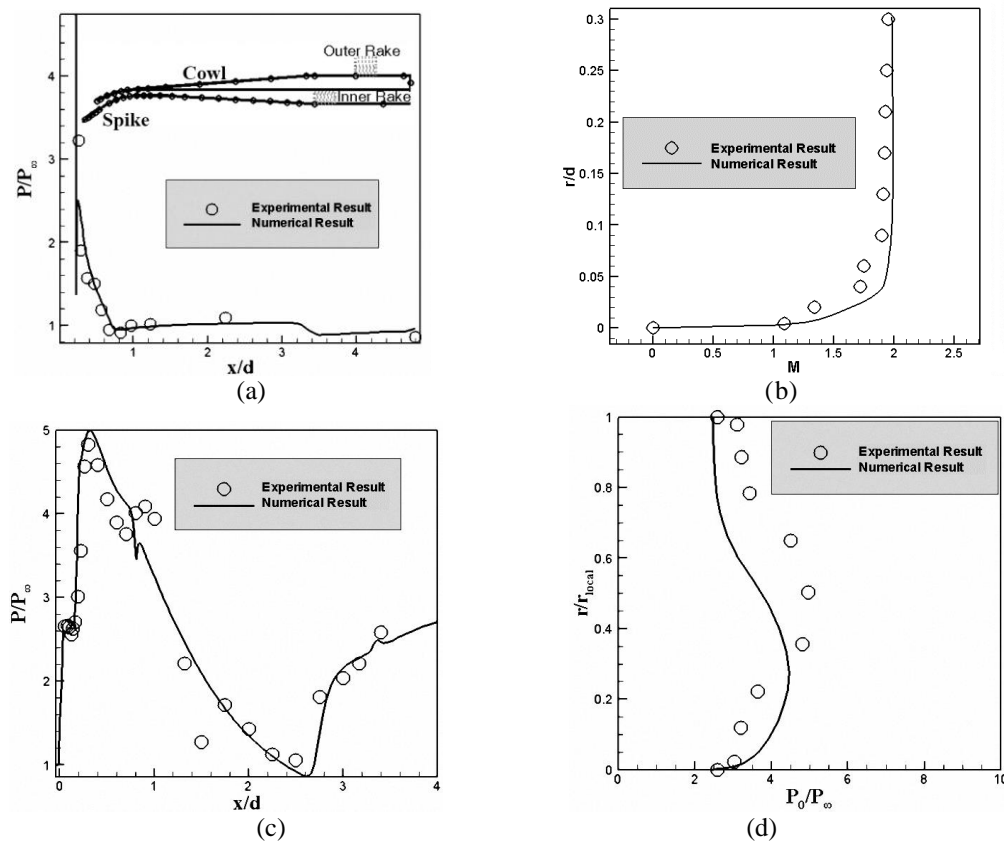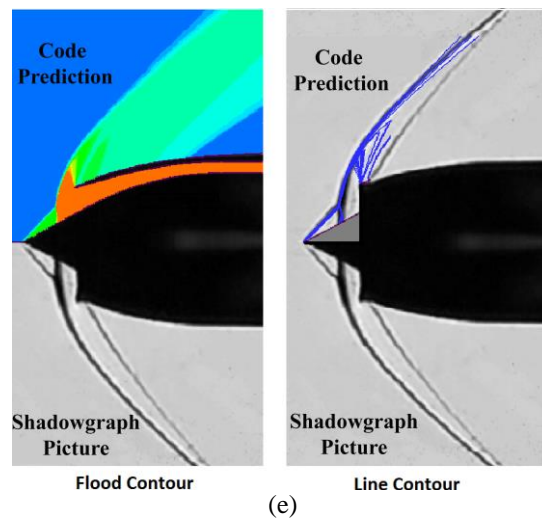

Fig. 5. Comparison of the Numerical and Experimental Data for Validation Intake at M_∞=2.0 [16, 18], a) Static Pressure Ratio Distribution on the Cowl, b) Mach Number Distribution from the Outer Rake (*r* is measured from the local wall), c) Static Pressure Ratio Distribution on the Spike, d) Total Pressure Distribution from the Inner Rake (*r* is measured from the local wall), e) Shock Structures

Figure 5 Continued.

(e)

3. RESULTS AND DISCUSSION

In this section the method of numerical investigation of the intake starting problem will be explained first followed by the starting behavior of the specified intake, which will be investigated. Finally, the sensitivity and effects of the intake throat area, cowl lip roundness and spike surface curvature upstream of the throat on the starting and performance of the intake will be studied.

a) Method of numerical investigation of the intake starting problem

The authors found that in the numerical simulation of the intake if the upstream Mach number is set to its design value, two in the present case, from the beginning of the numerical iterations when the solution is converged, the normal shock will be placed inside the intake, Fig. 6a, and it is interpreted that the intake has no starting problem. However, for the same intake geometry if the numerical simulation is begun from a Mach number lower than the design one and then approaches to the design Mach number, the normal shock will be placed outside the intake, Fig. 6b. In this way one can recognize the starting problem for a specified intake and the second approach is a correct mean to survey the intake starting problem. The reason is that during the flight, when the flight Mach number approaches the design Mach number of 2, a normal shock is placed first outside the intake. As the design Mach number is reached, if the intake has no starting problem then the normal shock will move inside the intake and will be placed in the intake throat or downstream of it. As a result, to survey the intake starting problem properly by a numerical code, the aforementioned procedure should be numerically followed. The subcritical condition must first be simulated and then the solution should approach the critical condition.
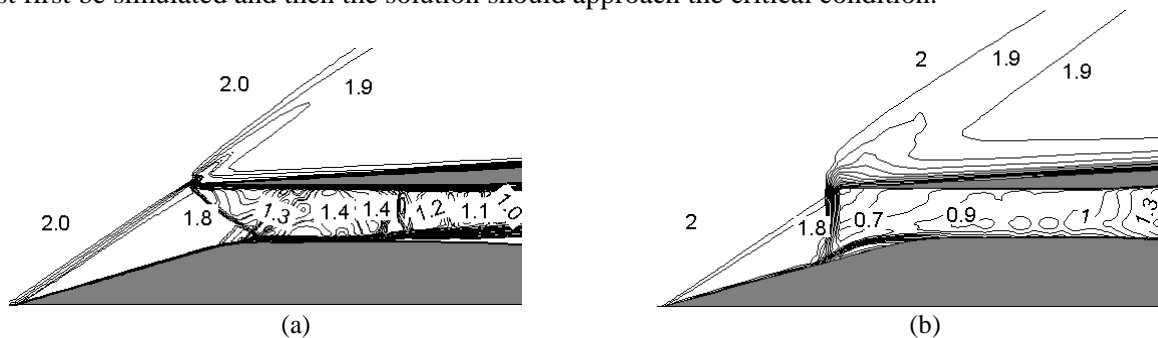

(a)   (b)

Fig. 6. Starting behavior of the intake (contours of Mach number) at $M_\infty=2.0$, a) $M_\infty=2.0$ from the beginning of the numerical iterations, b) $M_\infty<2.0$ for the start of iterations (iterations has begun from a Mach number lower than two and then approaches to two)

b) Effects of the intake throat area

The aforementioned method was used to survey the intake starting problem and the results showed that the starting Mach number of the base intake was 2.40 whilst its design Mach number was 2.0. Thus, to suppress the intake unstart problem, the intake throat area for eliminating the starting problem was investigated and the results are shown in Table 1. All variations used in Table 1 such as A_t, A_∞, and R_t are defined in Fig. 7. It is seen from Table 1 that the starting problem is very sensitive to the intake throat area.
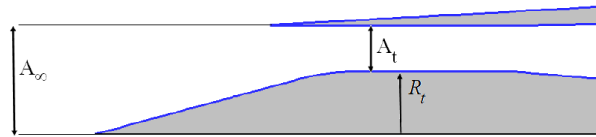

Fig. 7. Definition of the Intake Areas

Table 1. Effect of intake throat area on the starting Mach number

Reduction in R_t (mm)	A_t/A_∞	Increase in A_t (%)	Starting M_∞
0.0 (Initial Geometry)	0.661	0	2.40
0.50	0.689	4.4	2.15
0.65	0.697	5.6	2.10
0.75	0.703	6.4	1.80
1.00	0.716	8.5	1.80

The data of Table 1 shows that as R_t is reduced, A_t increases and the starting M_∞ decreases. By reducing R_t to 1 mm, an increase of about 8.5% in A_t, the starting M_∞ decreases to 1.80 and we chose this value for reduction in R_t to ensure that the intake will start at its design Mach number, $M_\infty=2.00$.

c) Effects of the cowl lip roundness

In all simulations up to this point, the cowl lip was quite sharp, but for the actual intake the cowl lip has a finite radius. Numerical simulations showed that rounding the cowl lip with a radius of 0.10 mm again causes the intake to face with the starting problem even with increasing the intake throat area by 8.5%. With this round cowl lip, the intake starting Mach number is 2.10. The reason for this behavior is the increased value of the intake mass flow rate once the cowl lip has been rounded. For the intake with sharp cowl lip the cowl leading edge point is A, Fig. 8a, while for the rounded one the leading edge is point B, Fig. 8b. Note that point A is fixed in space. In fact, changing the cowl lip leading edge point from A to B the intake mass flow rate will be increased slightly according to Fig. 8 (the streamlines were obtained from the numerical simulations) and this increase in the mass flow rate again leads to the intake unstart problem.
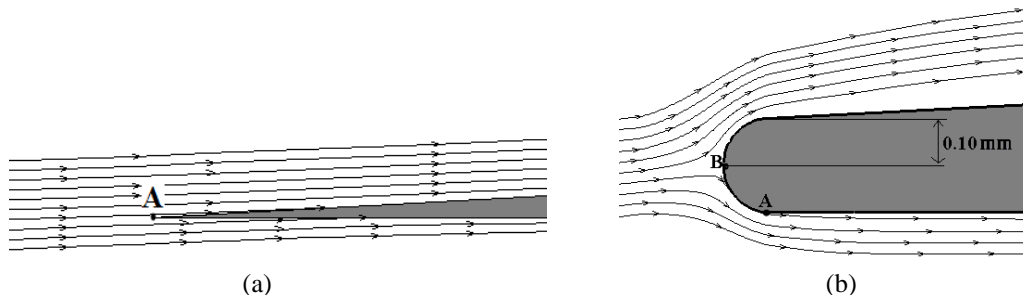

| (a) | (b) |

Fig. 8. Cowl Lip Geometry and Streamlines around it, a) Sharp Leading Edge, b) Round Leading Edge

To suppress the intake unstart problem for this situation the cone semi vertex angle, θ shown in Fig. 1a, is increased from 15° to 16° which will cause a slight flow spillage. This causes the conical shock

angle to increase from 34° to 34.6° and as a result, increases the flow spillage around the cowl lip that reduces the intake mass flow rate and leads to a starting Mach number of 2.00. Larger angle for the conical shock wave increases the shock stand off point, distance between the shock wave and the cowl lip, and as a result more mass flow rate can escape from this gap.

To prevent the increase in the intake mass flow rate for the rounded cowl lip, it is also possible to round the cowl lip in such a way that point A again becomes the leading edge point of the new cowl lip as shown in Fig. 9. However, in this way the height of the duct in the throat section of the intake is reduced and can cause the intake unstart due to the reduction in the throat area.

Fig. 9. New Cowl Lip Roundness

d) Effects of the spike surface curvature upstream of the throat

The effect of the spike surface curvature upstream of the throat on the starting behavior of the intake was also investigated. For this case, two surface fillets shown in Fig. 10 were examined. These fillets must join the cone surface with the surface of the throat. For fillet 1, the purpose was to restrict the cone angle to be 16°; however, for fillet 2 no restriction was applied and it was designed such that the flow would be smoothly directed toward the throat.
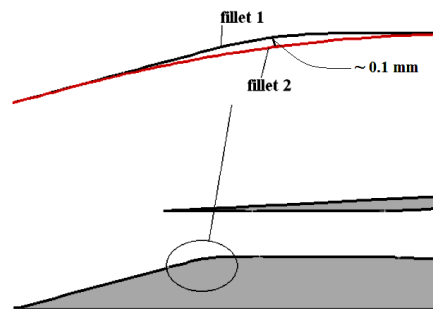

Fig. 10. Two Surface Fillets Upstream of the Throat

Numerical simulation of the intake with these fillets showed that the starting Mach number of the intake with fillet 1 was 1.95 and increased to 2.00 with fillet 2. In addition, as shown in Fig. 11, for the off designed Mach numbers the flow separation behind the normal shock with fillet 2 is more than that for the fillet 1 case which will degrade the intake performance. In fact, before the intake starts, at Mach numbers less than 2 in the intake with fillet 2 the flow behind the normal shock separates, which reduces the effective throat area and causes the intake to start at a greater Mach number as compared with the fillet 1 case.
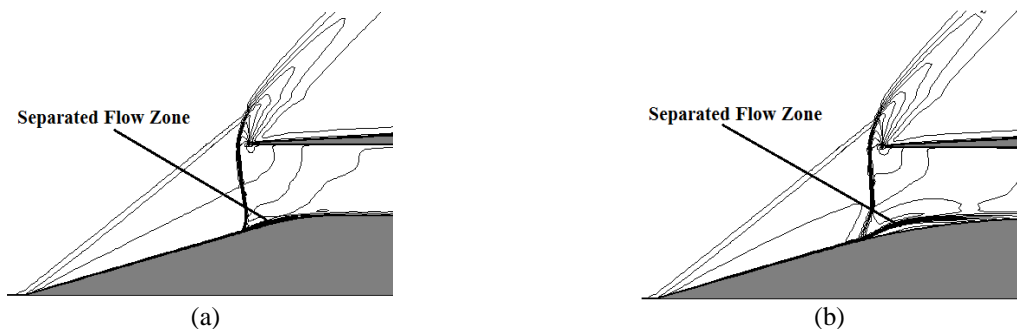

(a)   (b)

Fig. 11. Contours of Mach number at $M_\infty=1.75$, a) Fillet 1, b) Fillet 2

e) Intake performance analysis

In addition to the intake starting investigation the intake performance was studied to ensure that modifying the intake for the unstart suppression will not degrade the overall performance of the intake. Isolated intake performance is assessed by the TPR (Total Pressure Recovery), FD (Flow Distortion) and MFR (Mass Flow Ratio). Intake efficiency, TPR, is defined as the ratio of the mean value of the total pressure at the exit face of the intake to the free stream total pressure. The mass flow ratio, MFR, is defined as the ratio of the actual intake mass flow rate to the maximum mass flow rate that intake can capture [18]. Finally, flow distortion, FD, is defined as:

$$FD = \frac{\left(P_0\right)_{max} - \left(P_0\right)_{min}}{\left(P_0\right)_{avg}}. \tag{8}$$

It is desired for a supersonic air intake to have the maximum value of TPR and MFR and lowest possible FD.

Table 2 summarizes various geometries investigated in this study and Fig. 12 represents the corresponding performances for those geometries. The performance was calculated for the critical operation of the intake. In the critical condition, the normal shock stands downstream very close to the intake throat. All performance parameters shown in Fig. 12 are calculated for $M_\infty = 2.00$, however, for geometries that the intake starting Mach number was higher than 2.00, the numerical code was first run for the starting Mach number (higher than 2.00) and then the Mach number was reduced to $M_\infty = 2.00$. In this way, the normal shock was trapped in the vicinity of the intake throat and the critical condition at $M_\infty = 2.00$ was obtained. To locate the normal shock around the intake throat for the critical condition, a proper value for the static pressure at the pressure outlet boundary condition was set (Fig. 2). Note that the normal shock position in the intake at every Mach number is controlled by the static pressure in the exit face of the intake.

Table 2. Various intake geometries studied in this research

Case	Geometry Description
I	Base Geometry
II	Case I with an Increase in the Throat Area by 8.5%
III	Case II with a Rounded Cowl Lip
IV	Case III with a 16° Cone Semi Vertex Angle and with Fillet 2
V	Case IV but with Fillet 1 Only

According to Fig. 12a, the final geometry has the lowest starting Mach number. From Fig. 12b it is seen that when the intake throat area is increased, the starting problem diminishes; however, it reduces the intake efficiency which is not desired. In fact, as the intake throat area is increased the strength of the normal shock inside the intake increases and as a result the total pressure loss across the normal shock increases, a phenomenon that is responsible for decreasing the intake efficiency. The Mach number upstream of the normal shock for the case I intake is 1.30 and for the case II is 1.43.

Figure 12b also shows that rounding the cowl lip leads to an increase in the intake efficiency, case III. The reason for this situation is that rounding the cowl lip causes the formation of a stronger oblique shock around the lip, resulting in a shock train in the throat section being generated (Fig. 13). Thus, the normal shock that stands downstream of the shock train is weaker when compared with case II; as a result the total pressure loss across the normal shock is reduced.
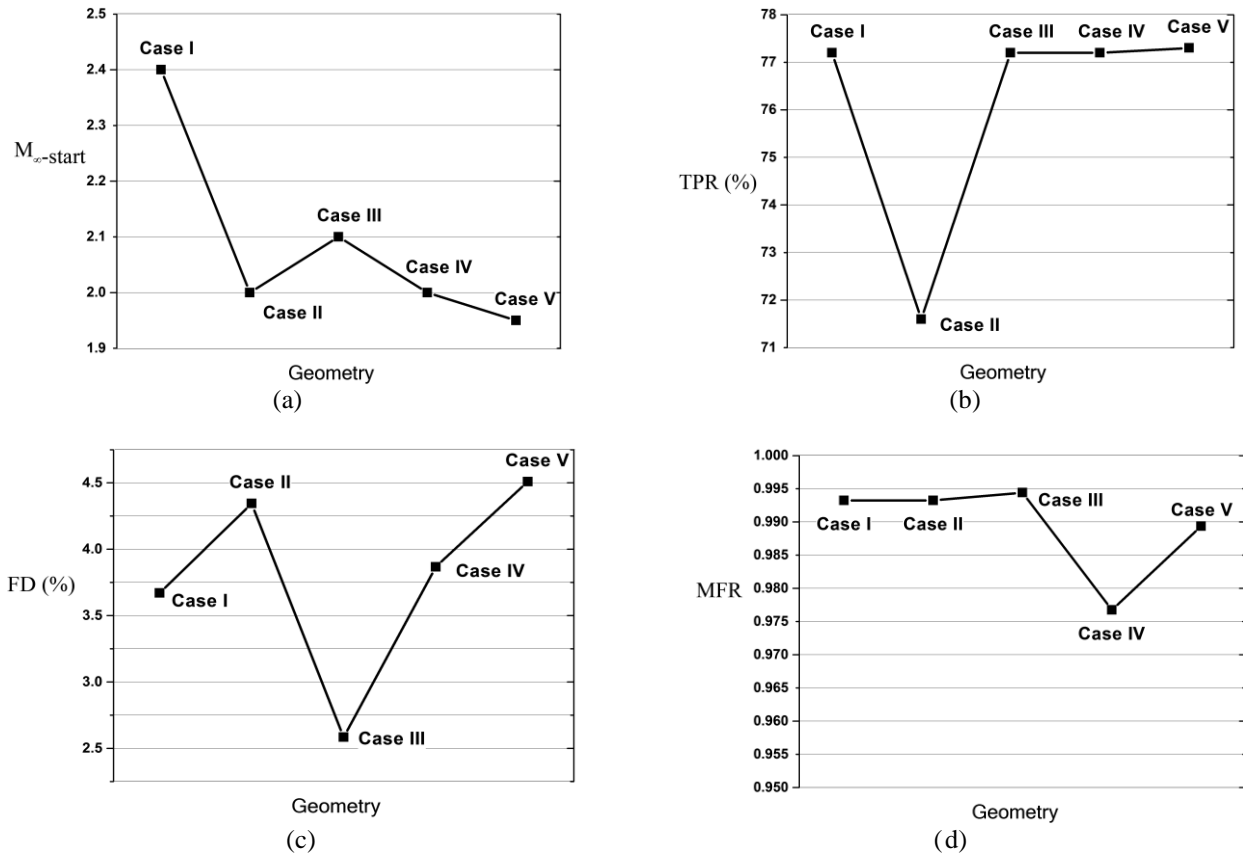
(a)

(b)

(c)

(d)

Fig. 12. Starting mach number and intake performance for various geometries, a) Free stream
starting Mach number, b) TPR, c) FD, d) MFR

(a)   (b)
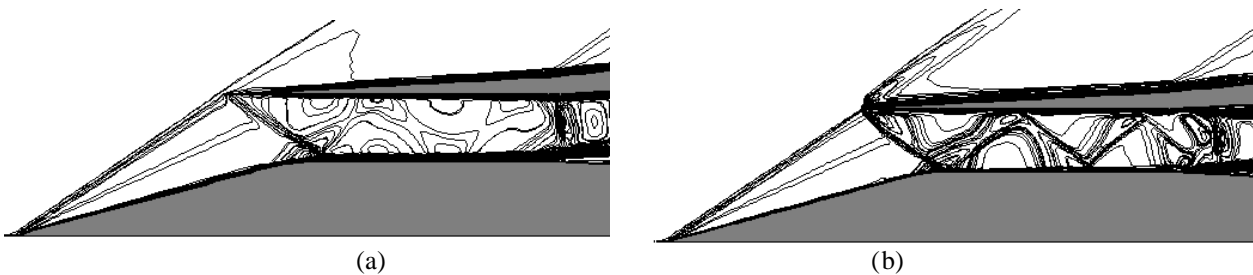
Fig. 13. Contours of Mach number at M_∞=2.00 at Critical Condition, a) Case II, b) Case III

In addition, it is seen from Fig. 12b that when the cone semi vertex angle is modified from 15° to 16°, the intake efficiency does not vary, however, the intake with fillet 1, case V has a higher efficiency when compared to the similar case, but with fillet 2, case IV. This is obviously due to the limited flow separation region with fillet 1.

Figures 12c and 12d show that the final geometry, case V, as compared with the base geometry, case I, has only 1% increment in the distortion and a small reduction of the MFR. Thus, it is concluded that the changes applied to the base intake do not degrade the intake performance significantly.

4. CONCLUSION

The starting characteristics of a supersonic mixed compression intake were studied via an existing numerical code that was throughly validated by a series of wind tunnel tests for a similar intake. Simulations of the intake flow field by this code showed that the base geometry of the intake has starting Mach number higher than the designed one. To resolve this problem, the intake throat area must be increased. However, increasing the intake throat area reduces the intake efficiency. To overcome this

situation, several modifications such as rounding the cowl lip, increasing the cone semi vertex angle, choosing a suitable spike surface curvature upstream of the throat were applied. These geometrical variations increased the intake efficiency. In summary, modifications proposed in this study changed the base intake with the starting Mach number of 2.40 and efficiency of 77.2% to an intake with the starting Mach number of 1.95 and an efficiency of 77.3% without any considerable performance reduction.

NOMENCLATURE

A	grid cell area, flow area
d	model diameter
E	total internal energy
F_c	convective flux vector
F_v	viscous flux vector
FD	flow distortion
H	total enthalpy
k	thermal conductivity coefficient
M	mach number
MFR	mass flow ratio
n	magnitude of the normal vector to the cell face
p	static pressure
P_0	total pressure
r	radial coordinate
s	length element along the cell face
T	static temperature
t	time
TPR	total pressure recovery
u	axial component of the velocity
v	radial component of the velocity
x	axial coordinate

Greek

Δ	change of variable
η	second coordinate in the computational domain
ρ	air density
τ	stress
ξ	first coordinate in the computational domain

Subscripts

c	convective flux
i, j	axial and radial counters of the grid cells
r	radial direction
n	normal direction of the cell face
v	viscous flux
x	axial direction
θ	circumferential direction, spike deflection angle

Superscripts

n	time level in discretization

REFERENCES

1. Hill, P. G. & Peterson, C. R. (1992). *Mechanics and thermodynamics of propulsion*. 2nd Ed., Addison-Wesley, New York, 1992, Chap. 6.

2. Seddon, J. & Goldsmith, E. L. (1985). *Intake Aerodynamics, An account of the mechanics of flow in and around the air intakes of turbine-engined and ramjet aircraft and missiles*. Collins, London, Chap. 6.

3. Kojima, T. & et al. (2004). Experimental Study on Restart Control of a Supersonic air-breathing Engine. *J. Propulsion and Power*, Vol. 20, No. 2, pp. 273–279.

4. Neiner, G. H. & et al. (1979). A throat-bypass stability-bleed system using relief valves to increase the transient stability of a mixed-compression inlet. NASA TP-1083.

5. Das, S. & Prasad, J. K. (2010). Unstart suppression and performance analysis of supersonic air-intake adopting bleed and cowl bending. *IE (I) Journal–AS*, Vol. 91, pp. 27-35.

6. Das, S. & Prasad J. K. (2010). Starting characteristics of a rectangular supersonic air-intake with cowl deflection. *The Aeronautical Journal*, Vol. 114 (1153), pp. 177-189.

7. Das, S. & Prasad, J. K. (2009). Cowl deflection angle in a supersonic air intake. *Defence Science Journal*, Vol. 59, No. 2, pp. 99-105.

8. Das, S. & Prasad, J. K. (2008). Characteristics of a supersonic air-intake with bleed. INCAST 2008- 070.

9. Kubota, Sh., Tani, K. & Masuya, G. (2004). Aerodynamic performances of the combined cycle inlet. 24th Int. Congress of the Aero. Sci., pp. 1-8.

10. Jain, M. K. & Mittal, S. (2006). Euler flow in a supersonic mixed-compression inlet. *Int. J. Numer. Meth. Fluids*, Vol. 50, pp. 1405–1423.

11. Kotteda, V.M. and Mittal, S., "Viscous Flow in a Mixed Compression Intake", Int. J. Numer. Meth. Fluids, 67 (11), 2011, pp. 1393-1417.

12. Sanders, B. W. & Mitchell, G. A. (1970). Increasing the stable operating range of a mach 2.5 inlet. NASA TM X-52799, 1970.

13. Najafiyazdi, A. (2007). Theoretical and numerical analysis of supersonic inlet starting by mass spillage. Master of Engineering Thesis, McGill University.

14. Slater, J. W. & Saunders, J. D. (2008). Modeling of Fixed-exit Porous Bleed Systems", AIAA Paper, AIAA–2008–0094.

15. Nori, V. N. (2003). Unsteady flow in a mixed compression inlet at mach 3.5. MS Thesis, University of Florida.

16. Soltani, M. R., Farahani, M. & Sepahi Younsi, J. (2011). Performance study of a supersonic inlet in the presence of a heat source. *Scientia Iranica B*, Vol. 18, No. 3, pp. 375-382.

17. Soltani, M. R., Sepahi Younsi, J. & Farahani, M. (2012). Investigation of a new flux scheme for the numerical simulation of the supersonic intake flow. *Proc. IMechE Part G: J. Aerospace Engineering*, Vol. 226, No. 11, pp. 1445-1454.

18. Soltani, M. R., Sepahi Younsi, J., Farahani, M. & Maseud, A. numerical simulation and parametric study of a supersonic intake. *Proc. IMechE Part G: J. Aerospace Engineering*, Vol. 227, No. 3, pp. 467-479.

19. Hoffmann, K. A. & Chiang, S. T. (2000). *Computational fluid dynamics*. Vol. 1, 4th Edition, Engineering Education System, Wichita, Chap. 9.

20. Blazek, J. (2001). *Computational fluid dynamics: principles and applications*. Elsevier Science, London, 2001, Chap. 4.

21. Gokhale, S. S. & Kumar, V. R. (2001). Numerical computations of supersonic inlet flow. *Int. J. Numer. Methods Fluids*, Vol. 36, pp. 597–617.

22. Smith, C. F. & Smith, G. E. (2005). Two stage supersonic inlet (TSSI): 10-inch model calculations. NASA/ CR-2005-213287.

23. Lu, P. J. & Jain, L. T. (1998). Numerical investigation of inlet buzz flow. *J. Propulsion and Power*, Vol. 14, No. 1, pp. 90–100.

24. Sakowski, B. & *et al*. (1992). Evaluation and application of the Baldwin-Lomax turbulence model in two-dimensional, compressible boundary layers. NASA, TM-105810.

25. Kumar, A. (1986). Numerical simulation of scramjet inlet flow fields. NASA Technical Paper no. 2517.

26. Soltani, M. R. & Farahani, M. (2012). Effects of angle of attack on the inlet buzz. *Journal of Propulsion and Power*, Vol. 28, No. 4, pp. 747–757.

27. Samimi, S., Davari, A. R. & Soltani, M. R. (2013). *Canard-wing Interactions in subsonic flow. Iranian Journal of Science & Technology, Transactions of Mechanical Engineering*, Vol. 37, No. M2, pp. 133-147.